

# Mesh-size insensitive turbulence modelling for the 2d shallow water equations

G.R. Collicutt, S. Gao & W.J. Syme  
*BMT, Brisbane, Australia*

**ABSTRACT:** Turbulence within rivers plays a significant role in determining the mean flow velocity field and is integral to the overall energy loss mechanism. With the continued advance of computational hardware, rivers are now frequently modelled in 2D (rather than 1D) using the depth-averaged Navier-Stokes equations (i.e. Shallow Water Equations), often with higher order schemes and sometimes at cell resolutions less than the flow depth. With this trend, some treatments of turbulent eddy viscosity can lead to mesh size dependency in the results and significant errors in the prediction of inundation levels on the surrounding floodplains. Investigations into the issue of mesh-size sensitivity and the convergence of model results to physical test data for five turbulence models were performed, utilising three benchmark case studies from laboratory to real-world scale. In each case model results were compared with calibration data, with emphasis on head loss predictions.

## 1 INTRODUCTION

### 1.1 *Primary flow paths*

During a significant flood event, the majority of the flow is carried within, or near to, the river or open channel system (the primary flow path), and the water levels on the surrounding floodplains are principally determined by the energy losses along this flow path. Manning's equation is accurate for straight or slowly varying channels but does not calculate energy losses due to sudden changes in flow direction or velocity, and it does not capture super-elevation at bends. One dimensional (1D) models of river systems require these additional energy losses to be manually added and determined through model calibration against known flood events, and they have difficulty in accurately representing the floodplain. Two (2D) and three dimensional (3D) hydraulic models are more capable of automatically capturing these energy losses, however, they are NOT guaranteed to do so. To automatically and accurately capture these additional energy losses, the scheme must be physics based with a turbulence closure model, carefully designed to reduce mesh size sensitivities and time-step sensitivity, and thoroughly benchmarked against appropriate test cases.

### 1.2 *Turbulence*

Turbulence causes near infinite detail within fluid flows, and in a chaotic way: from an initial fluid state there are an unlimited number of possible future states for which mass and momentum have been conserved. Turbulence also causes diffusion of momentum: it determines how bed friction is transported into the main body of flow (i.e. determines the velocity depth profile), and it determines how bank friction is transported horizontally into the main body of flow (i.e. the horizontal velocity profile). Fundamentally, by determining how the momentum of the primary flow is diffused out to the riverbanks and floodplains, turbulence and surface elevation become intractably linked.

There are three primary approaches to capture how turbulence diffuses momentum. The first is to use a sufficiently fine mesh to resolve all sizes of eddies, so that the diffusion process is captured directly in the solution field. This is known as direct numerical simulation (DNS), however, for most real-world water flows this requires using a sub-millimetre 3D mesh and is not practical for civil hydraulic modelling. The second approach is to use a model to represent the effect of eddies without explicitly capturing them in the flow solution. Such ‘eddy viscosity’ models can be divided into two broad categories. The first, known as Reynolds Average Stress, or RAS, attempt to capture the effect of eddies of all sizes, leaving the flow field looking very much like a time averaged flow field and devoid of spatial and transient detail. The second, known as Large Eddy Simulation, or LES, only models the effects of eddies that are too small to be explicitly captured by the mesh resolution. In the absence of other energy losses LES models exhibit a flow solution rich with spatial and transient detail.

### 1.3 The Problem

The problem that has become evident is that shallow flows of fluid exhibit both 2D and 3D behaviour and, when solving the 2D depth-averaged Shallow Water Equations (SWE), this has material bearing on the correct formulation of LES turbulence closure models. This research presents a discussion on the turbulent kinetic energy cascade within shallow flows, a selection of eddy viscosity models that were numerically trialled, a selection of benchmark hydraulic test cases, and a summary of the results. The TUFLOW™ HPC numerical scheme (Collecutt & Syme 2017) was used to examine the performance of the various eddy viscosity models.

## 2 TURBULENT KINETIC ENERGY CASCADE WITHIN SHALLOW FLOWS

Kolmogorov (Frisch 1995) proposed a mathematical description of the process in which the power spectral density of the turbulence within the inertial subrange remains in equilibrium as the energy flows from large scales down to Kolmogorov scales, where it is dissipated as heat by molecular viscosity. In Fourier space the power spectral density of the turbulence is proportional to the wave number to the power of  $-5/3$ , as shown in Figure 1(a) (Husted 2017). The inertial subrange within the energy cascade in Figure 1(a) is where the turbulence is in equilibrium regarding its internal structure. If additional sources/sinks of turbulent energy are present at scales within the inertial sub-range, then the relationship is broken, and the distribution may become bi- or multi-modal. Shallow fluid flows are an example of this. It is really

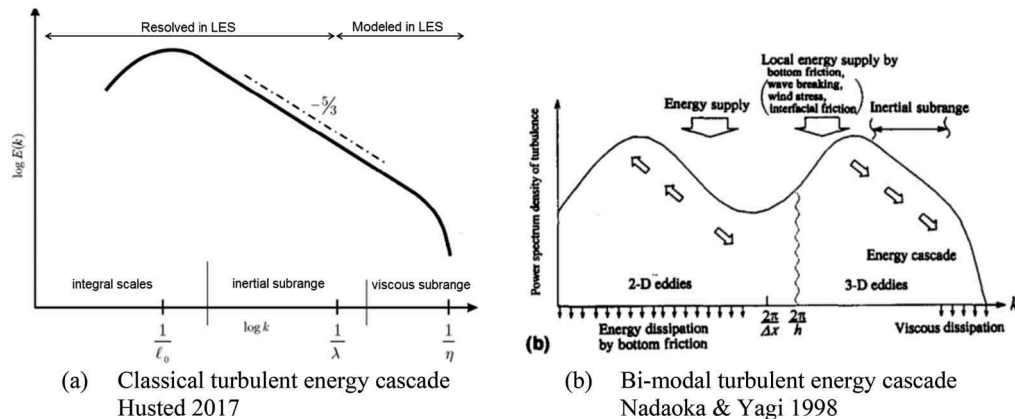


Figure 1. Classical and bi-modal turbulent energy cascades.

only on scales less than the fluid depth that the turbulence is free of sources and sinks, and a three dimensional standard energy cascade (down to the Kolmogorov scales) is formed. Nadaoka & Yagi 1998 offered an illustration of the bi-modal nature of the energy cascade, repeated here in Figure 1(b).

### 3 TURBULENCE CLOSURE FOR THE SWE

The 2D depth-averaged Shallow Water Equations, are shown in Equations 1 to 3.

$$\frac{\partial h}{\partial t} + u \frac{\partial h}{\partial x} + v \frac{\partial h}{\partial y} = S_h \quad (1)$$

$$\frac{\partial hu}{\partial t} + u \frac{\partial hu}{\partial x} + v \frac{\partial hu}{\partial y} = \frac{\partial}{\partial x} h \left( \nu \frac{\partial u}{\partial x} - \overline{u'u'} \right) + \frac{\partial}{\partial y} h \left( \nu \frac{\partial u}{\partial y} - \overline{u'v'} \right) - gh \left( \frac{\partial(z+h)}{\partial x} + \frac{n^2 |U| u}{h^{\frac{4}{3}}} \right) \quad (2)$$

$$\frac{\partial hv}{\partial t} + u \frac{\partial hv}{\partial x} + v \frac{\partial hv}{\partial y} = \frac{\partial}{\partial x} h \left( \nu \frac{\partial v}{\partial x} - \overline{v'u'} \right) + \frac{\partial}{\partial y} h \left( \nu \frac{\partial v}{\partial y} - \overline{v'v'} \right) - gh \left( \frac{\partial(z+h)}{\partial y} + \frac{n^2 |U| v}{h^{\frac{4}{3}}} \right) \quad (3)$$

where  $h$  is fluid depth,  $u$  and  $v$  are the two horizontal velocity components,  $x$  and  $y$  the respective horizontal coordinates,  $S_h$  the fluid source,  $\nu$  the laminar viscosity,  $u'$  and  $v'$  the fluctuating components of the velocities,  $g$  is gravity,  $z$  the bed elevation, and  $n$  the Manning's bed friction coefficient. The Boussinesq hypothesis is commonly used to replace the Reynold's stresses with an eddy viscosity as shown in Equations 4 to 6.

$$-\overline{u'u'} = \nu_t \left( \frac{\partial u}{\partial x} + \frac{\partial u}{\partial x} \right) - k \quad (4)$$

$$-\overline{u'v'} = \nu_t \left( \frac{\partial u}{\partial y} + \frac{\partial v}{\partial x} \right) \quad (5)$$

$$-\overline{v'v'} = \nu_t \left( \frac{\partial v}{\partial y} + \frac{\partial v}{\partial y} \right) - k \quad (6)$$

where  $\nu_t$  is the turbulent contribution to viscosity, also known as the eddy viscosity, and  $k$  is the turbulent kinetic energy, in this case  $(u'u' + v'v')/2$ . This inclusion of  $k$  in Equations 4 and 6 guarantees that the sum of the normal stresses in a flow of uniform depth is equal to  $2k$ . By using the Boussinesq hypothesis to model the Reynolds stresses as an eddy viscosity, the turbulence closure model must be carefully designed to capture the effect of turbulence that is not explicitly captured in the solution velocity field. For RAS simulations this may be virtually all scales of turbulence, but for LES simulations this is typically the sub-**grid**-scale turbulence. It is here that it must be recognized that the SWE are modelling in 2D what is essentially a 3D flow. A LES turbulence closure model assumes that as the cell size is reduced, the solution velocity field can represent turbulent structures of scales larger than the grid size. However, as discussed earlier, for shallow fluid flows 3D turbulent structures exist on scales less than the water depth, and these cannot be represented by a 2D velocity field. Therefore, once the grid size becomes similar to or smaller than the fluid depth, the effect of the 3D turbulence is not captured by either the 2D velocity field or the LES turbulence closure model. A possible, and simple, solution to this problem is to change the length scale filter for the LES model from the grid size to the fluid depth, so that the LES model becomes a sub-**depth**-scale turbulence model, rather than a sub-**grid**-scale turbulence model. This has already been proposed by Nadaoka & Yagi (1998). This proposition is that which is the primary subject of investigation regarding the selection of candidate eddy viscosity models.

## 4 EDDY VISCOSITY MODELS TRIALLED

Four eddy viscosity models were considered, as detailed below. They are all isotropic models, i.e. the turbulent diffusion of momentum is applied equally in all directions.

### 4.1 Constant

The first and simplest eddy viscosity model considered, as shown in Equation 7 (where  $v_t$  is the turbulent eddy viscosity), is where the eddy viscosity is assumed to be a constant throughout the domain. This approach was used extensively in coastal modelling applications for many years.

$$v_t = C \quad (7)$$

### 4.2 Smagorinsky

The second eddy viscosity model considered was the 2D Smagorinsky LES model as shown in Equation 8 where  $A$  is the cell area and  $|S_{2D}|$  the magnitude of the 2D velocity strain tensor, and  $u$  and  $v$  are the two horizontal velocity components.

$$v_t = MA|S_{2D}|; |S_{2D}| = \sqrt{\left(\frac{\partial u}{\partial x}\right)^2 + \left(\frac{\partial v}{\partial y}\right)^2 + \frac{1}{2}\left(\frac{\partial u}{\partial y} + \frac{\partial v}{\partial x}\right)^2} \quad (8)$$

### 4.3 Wu

The third model trialled was that of Wu *et. al.* (2004), as shown in Equation 9 where the turbulent eddy viscosity is the Pythagorean sum of two separate contributions. The first,  $v_{t2D}$ , is that of the larger scale 2D eddies, and the second,  $v_{t3D}$ , is that of sub-depth-scale 3D eddies.  $U^*$  is the friction velocity of the bed boundary layer,  $\tau_{bed}$  the bed shear stress, and  $\rho$  is density.

$$v_t = \sqrt{v_{t2D}^2 + v_{t3D}^2}; v_{t2D} = C_{2D}l_m^2|S_{2D}|; v_{t3D} = C_{3D}l_mU^*; U^* = \sqrt{\frac{\tau_{bed}}{\rho}} = \frac{|U|n\sqrt{g}}{h^{\frac{1}{6}}} \quad (9)$$

The friction velocity can also be expressed using the magnitude of the mean fluid velocity  $|U|$ , Manning's friction coefficient  $n$ , gravity  $g$ , and fluid depth  $h$ . In our application of this model, to create a **sub-depth**-scale turbulence closure model, the mixing length scale  $l_m$  is set to the minimum of water depth, or horizontal distance to the nearest dry boundary. This may not accurately represent the actual length scales for the 2D and 3D turbulence components, but it provides a length scale that the actual length scales should be approximately proportional to. The constants of proportionality then become part of the  $C_{2D}$  and  $C_{3D}$  coefficients. Of interest is that with  $l_m = h$ , the 3D contribution is an isotropic version of the passive transport diffusivity model (Lin & Falconer 1997).

### 4.4 Prandtl

The previous three models are all diagnostic models (in that the eddy viscosity can be computed from the instantaneous velocity field). The fourth and final model trialled was the one-equation Prandtl turbulence model commonly used for LES simulations (Wilcox 1994). This model is prognostic, requiring the transport and evolution of a single field parameter,  $k$ , representing the kinetic energy of the modelled turbulence per unit mass of fluid. In the application

at hand it is being used to represent the sub-**depth**-scale turbulence, by using a length scale in Equation 10 that is proportional to fluid depth, rather than the square-root-cell-area as might be used for a sub-**grid**-scale turbulence model. The kinetic energy of the modelled turbulence per unit mass of fluid, is evolved according to Equation 11. The production of turbulence is shown in Equation 12.

$$\nu_t = Mh\sqrt{k} \quad (10)$$

$$\frac{\partial hk}{t} + u \frac{\partial hk}{\partial x} + v \frac{\partial hk}{\partial y} = \frac{\partial}{\partial x} \left( \nu_t \frac{\partial kh}{\partial x} \right) + \frac{\partial}{\partial y} \left( \nu_t \frac{\partial kh}{\partial y} \right) + h \left[ P_k - C_D \frac{k^{\frac{3}{2}}}{Mh} \right] \quad (11)$$

$$hP_k = h\nu_t |S_{2D}|^2 + |U|U^{*2} \quad (12)$$

## 5 HYDRAULIC BENCHMARK CASES

Three benchmark cases were chosen, each with high quality test data sets allowing optimum eddy viscosity parameters for each model to be determined. Importantly the test cases span a wide range of scales and contain energy losses due to sudden changes in flow direction and velocity.

### 5.1 Right angled flume bend

Malone and Parr (2008) investigated the head losses associated with flow around sharp bends in rectangular section channels. Their test setup was at laboratory scales with a flume width of 150 mm and a comparable flow depth. An analysis of the 90-degree bend case yielded a loss factor in the range of 1.22-1.42 based on upstream velocity. The flume was reported as having a Manning's bed friction coefficient of close to 0.01.

### 5.2 Dam breach into channel with obstruction

Neelz and Pender (2010) published (through the UK Environment Agency) a range of benchmark hydraulic tests against which 2D SWE solvers were evaluated. One of the more challenging of the benchmark models was the case of a dam breach into a channel with an obstruction (Soares-Frazão & Zech 2002), otherwise known as Test 6A. The schematic for the test including gauge locations is shown in Figure 2. The channel was constructed of smooth concrete and reported to have a Manning's bed friction coefficient of 0.01. Regions of super-critical flow and hydraulic jumps were observed and six gauges measured water depth and velocity.

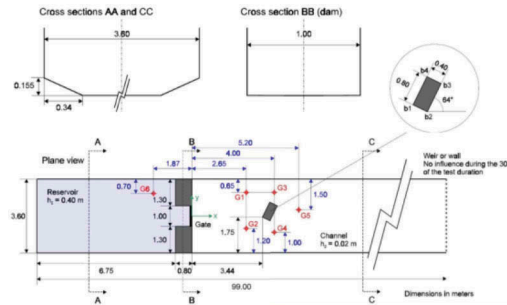


Figure 2. Schematic of UK EA Test 06A.

### 5.3 Large meandering river in bank-full flood

The third benchmark case is that of the Brisbane River (Australia) during the 2011 flood event. The river is tightly meandering and during the flood event was running at approximately bank-full capacity with some overbank flooding. The volume flow rate was well established at around  $9,000 \text{ m}^3/\text{s}$  with ADCP current profiling, and the water levels were measured at numerous locations along the river. The head loss along an 11 km section of river through the city had been measured to be 4.0 m at the peak of the flood (for a downstream boundary level of 2.7 m Australian Height Datum). The Manning's bed friction was 0.022 (BMT 2015). Importantly, at full flood the eddy viscosity model accounts for a significant fraction of the 4.0 m head loss.

## 6 RESULTS

### 6.1 Right angled flume bend

The various eddy viscosity models were trialled with the right-angled flume bend. Model coefficients were varied to obtain approximate calibration against test data, and mesh-size convergence of the results was considered. The results are shown in Figure 3. The plot abscissa is the mesh size in terms of the number of cells across the flume width, and the ordinate is predicted loss factor. The dashed black lines represent the upper and lower bounds of the measured loss factor. For the model titled Wu 2D component (Figure 3c), the 3D coefficient was set to zero and only the 2D parameter varied, and vice-versa for the model titled Wu 3D component.

The most significant observation is that while all models appeared to demonstrate mesh-size convergence, the Smagorinsky model consistently converged to the same (and incorrect) result regardless of the model parameter. The reason for this is that the Smagorinsky model, being a sub-grid-scale LES turbulence model applied to a 2D velocity field, fails to capture the momentum diffusion caused by physical 3D turbulence at the sub-depth-scale. The remaining models were all able to be calibrated for this test case, and their optimal parameters are summarised in Table 1.

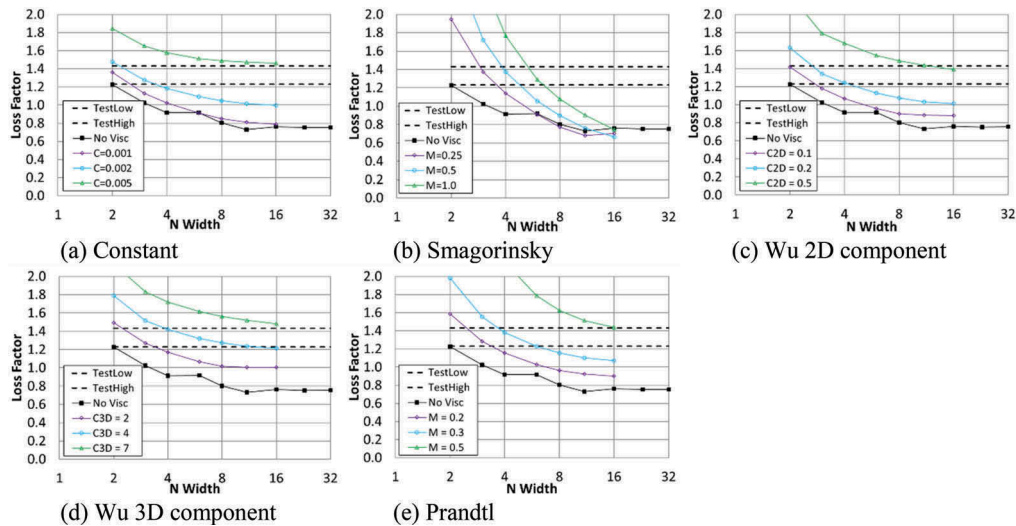


Figure 3. Mesh size converge of predicted loss factor for 90-degree bend, various viscosity models.

Table 1. Optimal eddy viscosity model coefficient.

Model	Constant [m <sup>2</sup> /s]	Smagorinsky [-]	Wu 2D [-]	Wu 3D [-]	Prandtl [-]
90 deg bend	0.004	No optimum	0.5	6	0.5
UK EA T06A	0.01	No optimum	0.4	3	0.4
Brisbane River	10	No optimum	4.0	7	1.0

### 6.2 Dam breach into channel with obstruction

The UK EA Test 6A case had 6 gauges installed, each recording water level and velocity. Gauge number 2 is of particular interest as the hydraulic jump that forms at the face of the obstruction gradually propagates upstream as the discharge slows and moves over the gauge during a period of 5 s from 15 to 20 s after the breach. The exact timing of this transition proved to be sensitive to the eddy viscosity model. An example comparison between test data and model result for depth and velocity for Gauge 2 are shown in Figures 4a and 4b. Mean square errors between test and model data were computed and normalized against mean depth/velocity for the 12 sets of data and summed. The total errors for the various eddy viscosity models as a function of cell size are shown in Figure 5. Again, all models bar Smagorinsky show a general trend for decreasing error with mesh size. Optimum values are summarised in Table 1.

### 6.3 Large meandering river in bank-full flood

Finally, the predicted head loss along the selected stretch of the Brisbane River (2011 flood event) is shown in Figure 6 as a function of mesh size for the various eddy viscosity models. Note that the actual recorded head loss was 4.0 m. Again, the Smagorinsky model is showing strong mesh size sensitivity, and converges to the same value regardless of model parameter. Optimum coefficients for the other models are summarised in Table 1. Interestingly Figures 6 (a), (c), (d) and (e) still show some evidence of mesh-size sensitivity which appears to be due primarily to the first order approach for computing cell volume storage and face flux area as functions of depth (i.e. flat bottomed cells and faces). This residual sensitivity can be mostly eliminated through the use of a higher-order approach for cell volume storage and face flux area as functions of depth (Kitts et. al. 2020) as shown for this case in Figure 6f.

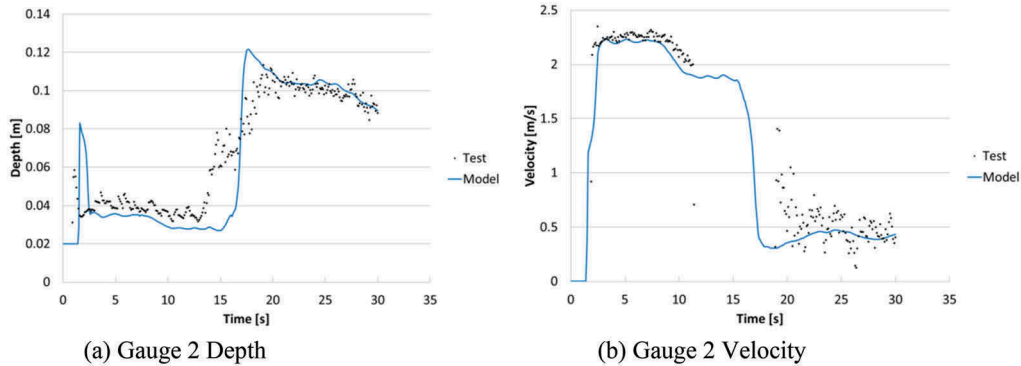


Figure 4. UK EA Test 06A, example test and model results.

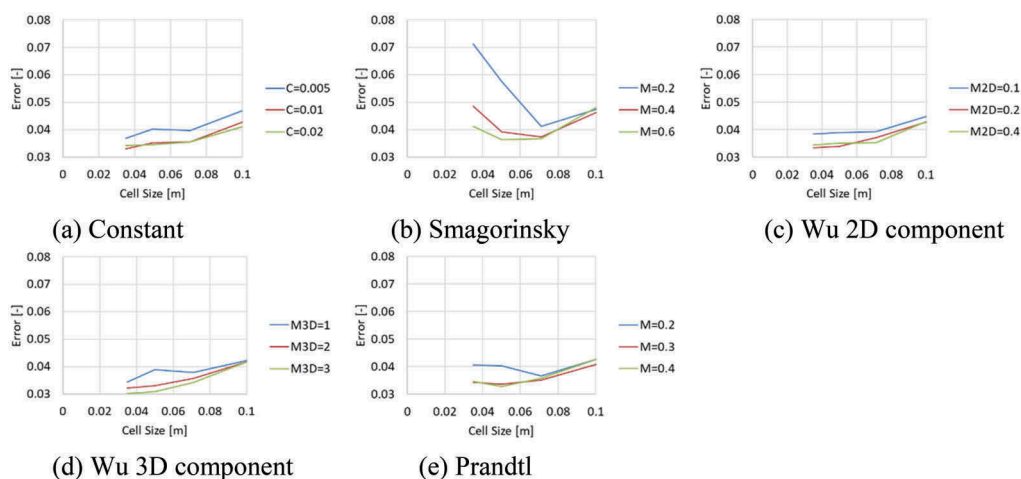


Figure 5. Mesh size convergence of total error for UK EA Test 06A, various viscosity models.

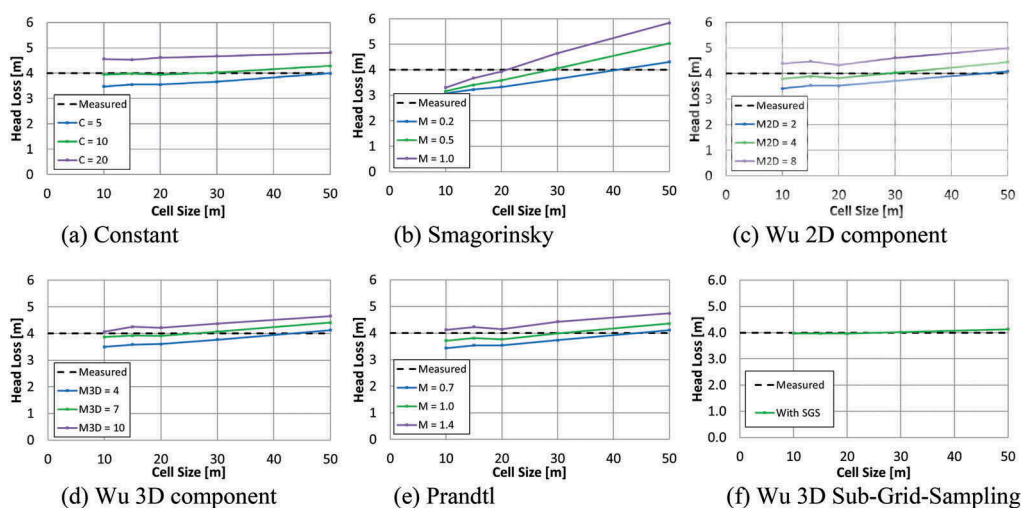


Figure 6. Mesh size convergence of head loss for Brisbane River model, various viscosity models.

#### 6.4 Summary of optimal model parameters

Table 1 summarises the optimum parameters for the five viscosity models considered and for the three benchmark hydraulic models. As already noted, the Smagorinsky model cannot be adjusted to converge to a sensible result as the mesh size is reduced. The remaining models can each be adjusted to achieve calibration for each of the benchmark cases. For the constant eddy viscosity model, the optimum parameter is highly sensitive to the physical scale of the problem. It is also likely to be sensitive to the magnitude of the flood event. The Wu 2D model shows a similar trend but not to the same extent. The Wu 3D and Prandtl models show the least sensitivity to scale, and therefore perform well at automatically and accurately capturing the head losses associated with turbulent viscosity. Interestingly the Wu 3D model, though a zero-equation formulation, appears to perform equally well to the Prandtl model for the cases studied.

## 7 CONCLUSIONS

A range of eddy viscosity models were trialled with benchmark hydraulic cases spanning a range of physical scales. In each case eddy viscosity played a critical role in determining head losses. The Smagorinsky model, formulated as a 2D sub-**grid**-scale LES eddy viscosity model, performed poorly at cell sizes similar to or smaller than the fluid depth. A possible explanation is that at these scales much of the eddy viscosity is caused by 3D turbulent structures that cannot be represented by either the 2D velocity field or the 2D sub-**grid**-scale LES eddy viscosity model. The constant eddy viscosity model, along with three sub-**depth**-scale LES eddy viscosity models all performed well. However, the constant eddy viscosity model was shown to have an optimum parameter that was strongly scale specific. The Wu 3D and Prandtl LES models, utilising length scale filters proportional to fluid depth, performed well across a range of model scales from small flume tests to large river scale with little change in optimum parameter.

## REFERENCES

- BMT 2015. Brisbane River Catchment Flood Study, Detailed Model Development and Calibration (Milestone Report 3) <https://www.publications.qld.gov.au/dataset/brisbane-river-catchment-flood-study/resource/16440193-2c27-45c6-850a-2ce1b1a30dd5>.
- Collecutt, G. & Syme W. 2017. Experimental benchmarking of mesh size and time-step convergence for a 1<sup>st</sup> and 2<sup>nd</sup> order SWE finite volume scheme. *Cambridge University Press ISBN 978-0-52145-103-1*.
- Frisch, U. & Kolmogorov, A. 1995. *Turbulence: The Legacy of A. N. Kolmogorov, ISBN 978-1-84911-190-4*.
- Husted, B. 2017. Turbulent Mixing in the Lower Part of the Smoke Layer using the Fire Dynamic Simulator, *1<sup>st</sup> International Symposium K-FORCE 2017*.
- Kitts, D. Syme, W. Gao, S. Collecutt, G. Ryan, P. 2020. Eliminating Mesh Orientation and Cell Size Sensitivity in 2D SWE Solvers. *Submitted paper for the IAHR 10<sup>th</sup> Conference on Fluvial Hydraulics, River Flow 2020, Delft, Netherlands*.
- Lin, B. Falconer, R. 1997. Tidal Flow and Transport Modeling using ULTIMATE QUICKEST Scheme, *Journal of Hydraulic Engineering, April 1997, pp 303-314*.
- Malone, T. & Parr. D 2008. Bend Losses in Rectangular Culverts, Kansas Department of Transport [http://ntl.bts.gov/lib/30000/30900/30935/KU-05-5\\_Final\\_Report.pdf](http://ntl.bts.gov/lib/30000/30900/30935/KU-05-5_Final_Report.pdf).
- Nadaoka, K. & Yagi, H. 1998. Shallow Water Turbulence Modeling and Horizontal Large Eddy Computation of River Flow, *Journal of Hydraulic Engineering, May 1998, pp 493-500*.
- Neelz, S. & Pender, G. 2010. Benchmarking of 2D Hydraulic Modelling Packages, UK Environment Agency, *ISBN 978-1-84911-190-4*.
- Soares-Frazão, S. & Zech, Y. 2002. Dambreak flow experiment: the isolated building test case. Technical Report, WP3 Flood Propagation, IMPACT (Investigation of Extreme Flood Processes and Uncertainty), EC Research Project No. EVG1CT2001-0037, [http://www.impact-project.net/wp3\\_technical.htm](http://www.impact-project.net/wp3_technical.htm) [Accessed 10th December 2019].
- Wilcox, D. 1994. *Turbulence Modeling for CFD, DCW Industries, Incorporated, 1994. ISBN 978-0-96360-510-8*.
- Wu, W. Wang, P. Chiba, N. 2004. Comparison of Five Depth Average 2D Turbulence Models for River Flows, *Hydro Engineering and Environmental Mechanics Vol 51 (2004) pp 183-200*.